Circulation Research

ORIGINAL RESEARCH

Human Hearts Intrinsically Increase Cardiomyocyte Mitosis After Myocardial Infarction

Robert D. Hume, Jessica Warwick, Woo Jun Shim, Cassandra Malecki, Mengbo Li, Lakshay Seth, Dylan Harney, Julien Dagher, Trina Lum, Geraldine Tierney, Wendy Cooper, Eugene Slaughter, Xiaosuo Wang, Lisa Nguyen, Louise Cole, James Edelman, Fairooj N. Rashid, Callum Houlahan, Antony Gao, Angela L. Ferguson, James J.H. Chong, Mark Larance, John F. O'Sullivan, Nathan J. Palpant, Paul Bannon, Sean Lal

BACKGROUND: Myocardial infarction (MI) is a leading cause of death worldwide and can eliminate up to a third of the cardiomyocytes within the human heart. Although cardiomyocytes undergo mitosis during early development, most cardiomyocytes cease cell cycling soon after birth. In contrast, rodent MI models have shown that cardiomyocytes increase mitosis in response to ischemia; however, this has not been shown in humans.

METHODS: Using a unique premortem post-MI human heart, immunostaining, bulk RNA sequencing, proteomics, metabolomics, single-nucleus RNA sequencing and a novel post-MI human biopsy method, we investigated human cardiomyocyte mitosis post-MI.

RESULTS: We show that adult human cardiomyocytes exhibit increased mitosis and cytokinesis in response to ischemia.

CONCLUSIONS: Future development of therapeutics to enhance this intrinsic mitotic potential could lead to new treatments that reverse heart failure via cardiac regeneration.

GRAPHIC ABSTRACT: A graphic abstract is available for this article.

Key Words: heart ■ ischemia ■ mitosis ■ myocardial infarction ■ myocytes, cardiac ■ regeneration

Meet the First Author, see p e000744

The adult human heart contains ≈3 billion cardiomyocytes. However, significant ischemic events, such as myocardial infarction (MI) caused by obstructive coronary artery disease, can eliminate up to a third of these cells.[1,2] Although survival after MI has improved over the past decade due to significant therapeutic advancements, many patients still develop irreversible heart failure.[3] Thus, identifying alternative options to prevent and reverse heart failure is paramount.

The tenet that the mammalian heart is a terminally differentiated organ in which cardiomyocytes lack the capacity to undergo mitosis has been challenged over the last decade.[1,4] For instance, several studies have demonstrated that nonhuman mammalian hearts have a considerable regenerative capacity during normal development.[2] Others have shown neonatal rodents can regenerate the apex of the heart after resection,[5] analogous to nonmammalian models.[1] However, after birth, the mitotic potential of cardiomyocytes decreases, with 1 study showing that human cardiomyocytes cease to produce daughter cells after 20 years of age.[6] In contrast to the uninjured adult heart, murine models of induced ischemic MI injury have demonstrated increased cardiomyocyte mitotic capacity in the peri-ischemic border

Correspondence to: Robert D. Hume, PhD, Johns Hopkins Dr, Charles Perkins Centre, School of Medical Sciences, Faculty of Medicine and Health, University of Sydney, Sydney, New South Wales 2050, Australia, Email robert.hume@sydney.edu.au; or Sean Lal, MD, PhD, Johns Hopkins Dr, Charles Perkins Centre, School of Medical Sciences, University of Sydney, Sydney, New South Wales 2050, Australia, Email sean.lal@sydney.edu.au

Supplemental Material is available at https://www.ahajournals.org/doi/suppl/10.1161/CIRCRESAHA.125.327486.
For Sources of Funding and Disclosures, see page 381.

ORIGINAL RESEARCH

Novelty and Significance

What Is Known?

- Previous adult rodent studies have shown that cardiomyocytes, the heart's muscle cells, show increased mitosis after myocardial infarction.
- Although this increased mitosis is too low to regenerate lost cardiac tissue, it shows adult rodents have an intrinsic regenerative potential.
- This increased cardiomyocyte mitosis postmyocardial infarction, however, has not yet been shown in human hearts.

What New Information Does This Article Contribute?

- The adult human heart has the potential to regenerate in an ischemic environment.
- We developed a novel adult human myocardial postinfarction biopsy method that allows collection of live cardiac tissue from the left ventricle infarct border zone (peri-ischemic) and remote zone (nonischemic).
- Using a unique infarcted adult human heart and these aforementioned infarct biopsies, we show adult human ventricular cardiomyocytes have increased intrinsic mitosis after myocardial infarction.

Within this study, we utilized a unique infarcted human heart and novel infarct biopsy technique, together with immunohistochemical and multiomics analyses, to reveal that the human heart increases cardiomyocyte mitosis after myocardial infarction. This is the first human study that proves what has previously been demonstrated in animal studies over the last 25 years. Importantly, future therapeutic development to amplify this intrinsic regenerative potential could provide new strategies to regenerate damaged human hearts, improving the lives of millions of heart failure patients worldwide.

Nonstandard Abbreviations and Acronyms

AURKB	aurora kinase B
BZ LV	peri-ischemic infarct border zone left ventricle
CABG	coronary artery bypass grafting
DAPI	4′,6-diamidino-2-phenylindole
ECM	extracellular matrix
HMG-CoA	β-hydroxy β-methylglutaryl-coenzyme A
IMC	imaging mass cytometry
MI	myocardial infarction
MI LV	ischemic left ventricle
MI RA	nonischemic right atrium
MI RV	partially ischemic right ventricle
MKLP1	mitotic kinesin-like protein 1
PCM1	pericentriolar material 1
pH3	phospho-histone H3
RNAseq	RNA sequencing
RZ LV	nonischemic healthy remote zone left ventricle
snRNAseq	single-nucleus ribonucleic acid sequencing
WGA	wheat germ agglutinin

zone.[7,8] Although these well-established rodent MI models of cardiac regeneration have been used for decades, there is no robust evidence that the observed post-MI increase in cardiomyocyte mitosis translates to humans. Indeed, there is an urgent need to regenerate the field of human cardiac regeneration itself.[9]

Here, we demonstrate that human hearts increase cardiomyocyte mitosis when stimulated by post-MI ischemia. To achieve this, we analyzed a unique premortem ischemic human heart using a multimodal approach of imaging mass cytometry (IMC), immunohistochemistry, multiomics, and single-nucleus RNA sequencing (snRNAseq). Together, these approaches measured both cardiomyocyte mitosis and cytokinesis and characterized the expression of myocardial transcripts, proteins, and metabolites within this unique heart. In addition, we demonstrated increased mononucleated cardiomyocytes, polyploidy and DNA damage within this unique heart. We also developed a novel method to obtain human heart biopsies from patients 7 to 10 days post-MI, which, after immunohistochemistry analyses, further confirmed that human cardiomyocytes show increased mitosis in response to ischemia.

METHODS

Data Availability

Raw data and related codes for analysis have been uploaded to publicly accessible repositories. Please see the Major Resources Table and Data and Code Availability in the Supplemental Material for details.

A detailed description of the methods and materials can be found in both the Supplemental Methods and the Major Resources Table within the Supplemental Material. All incubations were at room temperature unless stated otherwise.

Human Heart Tissue

Donor hearts (Sydney Heart Bank, University of Sydney) deemed suitable for heart transplantation but unable to be transplanted (for reasons including transportation logistics,

immune incompatibility, and donor-recipient mismatch in size) were procured, as previously described.[10] These are not postmortem samples. These nondiseased donor heart samples were from patients with a noncardiac cause of death and no significant comorbidities or cardiac risk factors (hence why the hearts would otherwise have been used for transplant). All hearts (nondiseased donor or ischemic) underwent formal pathological examination by clinical anatomic pathology to confirm either normal histological architecture or ischemic heart disease, respectively. Left ventricle (LV) samples were obtained immediately after harvest and snap-frozen in liquid nitrogen (−196 °C). The study was approved by the Human Ethics Committee of The University of Sydney (USYD No. 2021/122).

Procurement of a Unique Infarcted Human Heart

The unique infarcted human heart was acquired from a 48-year-old male patient, originally on the national donor list, who suffered a catastrophic acute MI due to a full occlusion of the left anterior descending artery. This patient had a cardiac arrest at the Royal Prince Alfred Hospital, Sydney, whereby a coronary angioplasty and stent insertion could not be achieved. The patient was then kept on life support for 5 days post-MI, at which point no neurological activity was detected and the patient was declared brain-dead. As the heart could not be used for transplant purposes, the next of kin kindly agreed to organ donation for research. The heart was then collected premortem and cryopreserved within 15 minutes; that is, fragments from the nonischemic right atrium (MI RA), partially ischemic right ventricle (MI RV) and ischemic LV (MI LV) were flash frozen and stored in liquid nitrogen, or fixed in 10% neutral buffered formalin (HTS012; Sigma) overnight, before use.

IMC Immunostaining

All IMC methods were modified to suit paraffin-embedded tissue from our previous frozen section immunostaining protocol.[11] Briefly, 7 µm sections were cut from paraffin-embedded tissue blocks. Sections were then dewaxed, rehydrated, underwent antigen retrieval, permeabilized and blocked for 1 hour at room temperature, followed by overnight incubation in 75 µL of IMC metal conjugated antibody cocktail per section. Iridium DNA intercalator diluted in PBS (1:300) was added, incubated for 30 minutes, washed in PBS, dipped 3× in ultrapure H_2O, air dried, and then stored in an air-tight container before imaging on an IMC with a Hyperion Imaging System (Fluidigm).

Immunohistochemistry for Frozen Sections

Snap-frozen cardiac fragments were mounted directly in optimal cutting temperature and cryo-sectioned at −20 °C into 12 µm or 50 µm sections using a cryostat (NX50 Cryostar Epredia). Sections were collected onto VWR Superfrost Plus charged glass microscopy slides. Sections were air dried (10 minutes), fixed in 10% neutral buffered formalin (15 minutes), washed 3× (5 minutes, wash buffer: 0.01% Triton-X 100-PBS), quenched in 0.1 mol/L glycine (10 minutes), permeabilized in 0.5% Triton-X 100 in PBS (10 minutes), washed 3× (5 minutes) and blocked in blocking buffer (1 hour, 5% normal donkey serum-5% acetylated bovine serum albumin (BSA)-0.01% Triton-X-PBS). Tissue was then immunostained with primary antibodies (Major Resources Table in Supplemental Material) diluted in blocking buffer (overnight, on a shaker, 4 °C). Tissue was washed (3×5 minutes) and incubated in secondary antibodies (Major Resources Table in Supplemental Material) diluted in blocking buffer (1 hour on a shaker, protected from light). Tissue was then washed (3×5 minutes), incubated in DAPI (4′,6-diamidino-2-phenylindole; 1 µg/mL, No. 62248; Thermo Fisher) with WGA (wheat germ agglutinin)-AlexaFluor555 (5 µg/mL, No. W32464; Thermo Fisher) in PBS for 1 hour and washed (3×5 minutes) before mounting and imaging on an inverted confocal microscope.

Bulk RNA Sequencing

Approximately 50 mg of tissue/sample was disrupted using a metal bead (No. 69989; Qiagen) in a 2 mL tube with 500 µL TRIzol (No. 15596018; Ambion) using the TissueLyser LT (Qiagen), and RNA extraction was performed according to TRIzol manufacturer's instructions. DNA removal was performed using Qiagen RNAse-Free DNase kit (No. 79254; Qiagen) and purified using the RNeasy Mini kit (No. 74104; Qiagen) according to the manufacturer's instructions. RNA quality was evaluated using a Nanodrop and an RNA Nano Chip (no. 5067-1511; Agilent) on an Agilent Bioanalyzer. Libraries were prepared with Illumina Stranded Total RNA prep Ligation with Ribo Zero Plus kit, according to the manufacturer's instructions. Libraries were sequenced using a paired-end 250 bp Illumina NovaSeq 6000 S4 flow cell.

Proteomics

Approximately 10 mg of powdered frozen heart tissue was homogenized in 4% sodium deoxycholate (No. D6750; Sigma) and 100 mM Tris-HCl pH 7.5. Samples were denatured at 95 °C, sonicated using QSonica R2 (QSonica) at 70% amplitude, centrifuged (18 000*g*), and supernatant collected. Next, a bicinchoninic assay (No. 23225; Thermo Fisher) was used to determine protein concentration and 20 µg of protein was digested using trypsin overnight at 37 °C before mass spectrometry preparation as described previously.[12] Peptides were injected onto a 30 cm x 70 µm C18 (Dr Maisch, Ammerbuch, Germany, 1.9 µm particle size) fused silica analytical column with a 10 µm pulled tip, coupled online to a nanospray ESI source. To resolve peptides, samples were run over a gradient from 5% to 40% acetonitrile for 120 minutes (flow rate 300 nL/min). Peptide electrospray ionization was performed at 2.3 kV. Next, MS/ms analysis was performed using a Q-Exactive Fusion Lumos mass spectrometer (Thermo Fisher; 27% normalized higher-energy collisional dissociation collision energy for fragmentation). Spectra were attained in a Data-Independent Acquisition using 20 variable isolation windows. Statistics analyses on both proteomics and RNAseq data were performed in RStudio (v4.2.2).

Metabolomics

Metabolomic protocols were modified from our previously published protocols.[13,14] 50 mg of tissue was lysed in a 2 mL round-bottomed tube with 6 µL per 1 mg tissue of extraction

medium (MeOH:$CHCl_3$, 2:1, v:v, No. FSBA456-4; Thermo Fisher and No. 650498; Sigma) and a metal bead, using a TissueLyser LT for 4×50 cycles, cooling on ice between cycles. After removing metal beads, samples were incubated on ice for 30 minutes. Then 2 µL $CHCl_3$ per 1 mg tissue was added and vortexed for 1 minute, followed by 2 µL of high-performance liquid chromatography H_2O (No. FSBW6-4; Thermo Fisher) per 1 mg tissue with 1 minute vortexing. Samples were centrifuged at 14 000 revolutions per minute (rpm) for 20 minutes at 4 °C, and the aqueous layer was transferred into a new microfuge tube. Next, 20 µL of aqueous layer was added to 80 µL of hydrophilic interaction liquid chromatography isocratic separation-single standard (10 mM L-Phenylalanine-d8; Cambridge Isotope Lab No. DLM-372) and 10 mM L-Valine-d8 (No. 486027; Sigma) in acetonitrile:MeOH (75:25, v:v, Optima LC-MS grade, No. A955-4 and No. A456-4; Fisher Scientific) for hydrophilic interaction liquid chromatography analysis or 40 aqueous with 60 µL of amide isocratic separation-single standard (10 mM L-Phenylalanine-d8, 10 mM thymine-d4 [No. 487066; Sigma], 10 mM citrate-d4 [No. 485438; Sigma] in acetonitrile:MeOH [75:25, v:v]) for AMIDE analysis, vortexed briefly then spun at 14 000 rpm for 20 minutes at 4 °C. The surface 90 µL was transferred into glass vials with glass inserts (Nos. 186000273 and WAT094179; Waters) for liquid chromatography-tadem mass spectrometery metabolite analysis.

Single-Nucleus RNA Sequencing

Tissue samples were dissociated into single nuclei using the 10x Chromium Nuclei Isolation Kit (No. PN-1000493; 10X Genomics) protocol for Single Cell Gene Expression and Chromium Fixed RNA Profiling. Samples were then loaded into a Chromium Next GEM Chip G (No. PN-1000127; 10X Genomics) for an output of 10 000 nuclei per sample. The library preparation was done according to Chromium Next GEM Single Cell 3′ Reagent Kits v3.1 Dual Index protocol. Quality control was done with Agilent 4200 TapeStation system. The cDNA libraries were sequenced on an Illumina (NovaSeq 6000, S1 100 cycle Flowcell) instrument at a depth of 200 million reads/sample (or 20 000 reads/cell). Sequencing was performed at the Rammaciotti Center for Genomics, University of New South Wales, Sydney.

Procuring Post-MI LV Biopsies From Patients With MI Undergoing Coronary Artery Bypass Graft Surgery

Consultants from the Royal Prince Alfred (Sydney) cardiothoracic team consented appropriate patients for this study. Regional hospital Human Research Ethics Committee approval was obtained (no. X14-039). Broad inclusion criteria were patients (male or female, age >20 years old) admitted to our hospital with a MI, where subsequent coronary angiography demonstrated coronary artery disease that required inpatient coronary artery bypass grafting (CABG), and participants consented. Epicardial biopsies were obtained under direct visualization during CABG from the LV peri-infarct border zone (peri-ischemic infarct border zone LV zone [BZ LV]) and normal nonischemic LV (nonischemic healthy remote zone LV zone [RZ LV]). Tissue was then frozen in optimal cutting temperature for downstream immunohistochemistry.

Statistical Methods

For full details of the statistical methods, please see the Supplementary Material. Briefly, for IMC cell cluster proportions, an unpaired Student *t* test was performed. Immunohistochemistry and microscopy analyses *P* values were calculated using a 1-way ANOVA test with Tukey multiple comparison test. Omics differential expression and pathway analyses used *P* values adjusted using the Benjamini-Hochberg method. For snRNAseq, statistical testing the significance of the enrichment, Fisher exact test (2-tailed) was used. For snRNAseq differential gene expression, a Wilcoxon rank-sum test (2-tailed) was applied, differential expression was DE were defined as false discovery rate<0.05 and average log2-fold change>0.5, and multiple testing correction was performed using Bonferroni-adjusted *P* values.

RESULTS

Characterization of a Unique Premortem Infarcted Human Heart

We obtained a unique infarcted human heart from a 48-year-old male patient who had an acute MI, secondary to complete occlusion of the left anterior descending coronary artery. This patient was sustained on life support for 5 days post-MI, but after displaying no neurological activity, their consented heart donation was premortem cryopreserved within 15 minutes of harvest. Regions of the LV (denoted MI LV), right ventricle (denoted MI RV) and right atrium (denoted MI RA) were collected, providing both ischemic samples (MI LV and MI RV) and nonischemic internal control samples (MI RA; Figure 1A). It should be noted that although the MI RV was subtended by a nondiseased right coronary artery, the left anterior descending coronary artery had the potential to cross the interventricular septum and partially supply the RV. Indeed, we observed ischemia within MI RV, albeit to a lesser degree than the MI LV. Throughout the study, we also utilized age- and sex-matched healthy donor LV premortem cryopreserved samples (denoted Donor LV), as external nonischemic controls.

To characterize the infarcted heart, we first performed histology, multiphoton second harmonic generation microscopy and immunohistochemistry. As with post-MI murine models, the ischemic MI LV showed replacement fibrosis, increased endothelial cells, and immune cell infiltration (Figure 1B through 1E; Figure S1). Next, we defined the cellular composition of the post-MI heart using an 18-antibody IMC panel with a machine learning multicut cell segmentation methodology.[11] This allowed identification of cardiomyocyte

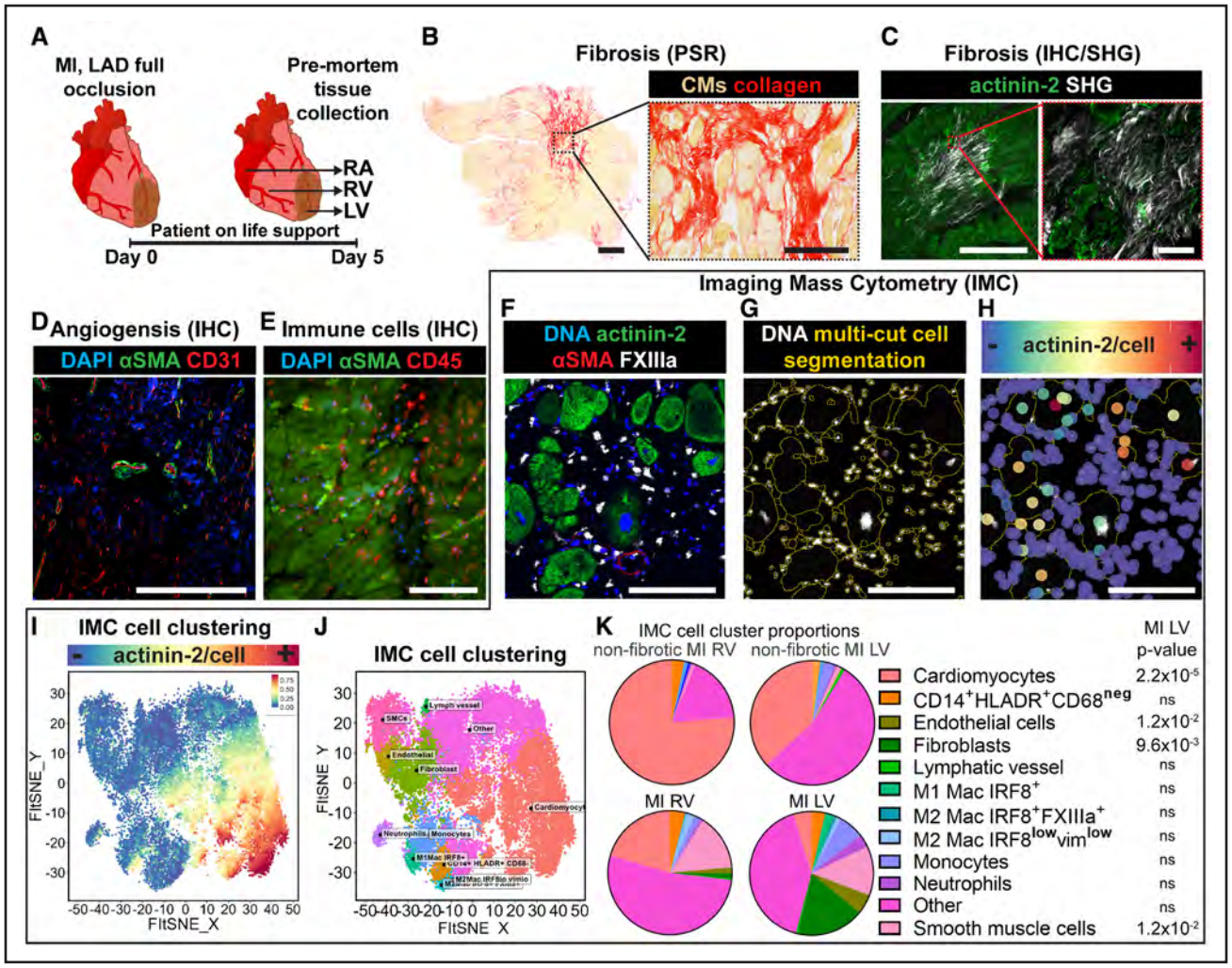

Figure 1. Characterization of a unique premortem infarcted human heart with left anterior descending coronary artery (LAD) occlusion.

The patient experienced complete LAD occlusion with subsequent myocardial infarction (MI). Five days post-MI, right atrium (nonischemic right atrium [MI RA]), right ventricle (partially ischemic right ventricle [MI RV]) and left ventricle (ischemic left ventricle [MI LV]) tissue were collected premortem for analyses. **A**, Tissue collection schematic. **B**, MI LV picrosirius red (PSR) staining (collagen, red; myocardium, yellow). **C**, Maximum intensity projection of optically cleared MI LV fragment with immunohistochemical (IHC) staining of cardiomyocyte (CM) sarcomeres (α-actinin-2, green) and second harmonic generation (SHG, white) of collagen. **D** and **E**, MI LV IHC showing increased (**D**) αSMA (α-smooth muscle actin; green) cells, CD31 (red) cells, and (**E**) immune cells (CD45, red), compared with nonischemic Donor LV. **F** through **K**, Imaging mass cytometry (IMC) with (**F**) representative image of MI LV with FXIIIa (factor XIIIa, white) immune cells, (**G**) cell segmentation, (**H**) segmented α-actinin-2 expression/cell, (**I**) α-actinin-2 expression/cell in t-distributed stochastic neighbour embedding (tSNE) unbiased IMC cluster analysis, (**J**) labelled IMC clusters, (**K**) Cell cluster proportions (unpaired Student *t* test of MI LV vs Remote LV, HLA-DR [human leukocyte antigen-DR isotype], Mac [macrophage], IRF8 [interferon regulatory factor-8]). Scale bars: **B**=1 mm/100 μm insert, **C**=500 μm/20 μm insert, **D**=500 μm, **E** through **H**=100 μm. DAPI indicates 4′,6-diamidino-2-phenylindole; and ns, not significant.

and noncardiomyocyte cell borders and analyzed relative protein expression within each cell (Figure 1F through 1H). Unbiased clustering of IMC analysis of segmented cells[11] revealed decreased cardiomyocytes and increased endothelial cells, fibroblasts, and smooth muscle cells within the MI LV (n=7), as compared with nonfibrotic areas (n=7) within the same infarct samples (denoted nonfibrotic MI LV, Figure S2; Figure 1I through 1K). These data show that this unique human heart exhibits similar structural and cellular post-MI remodeling to commonly utilized MI mouse models.[15]

Evidence of Increased Human Cardiomyocyte Mitosis in the Post-MI Heart

Increased cardiomyocyte mitosis has previously been reported in post-MI mouse models.[7,8] To confirm whether the human heart yielded similar results, we performed immunohistochemistry analyses. Within MI LV, we observed cardiomyocyte nuclei undergoing karyokinesis (Figure S3A). We also observed nuclear localization of S/G2/M-phase (early mid) mitosis marker pH3 (phospho-histone H3) within MI LV cardiomyocytes, identified by their α-actinin-2+ sarcomeres, WGA+

basement membrane or PCM-1+ (pericentriolar material 1) nuclei, with pH3+ cardiomyocytes observed in prophase, metaphase, and anaphase (Figure 2A and 2B; Figure S3B through S3E). Image analysis demonstrated increased pH3+ cardiomyocytes in MI LV, as compared with nonischemic internal (MI RA) and external (Donor LV) controls (Figure 2C). In addition, we observed G2/M-phase (mid-late) mitosis marker AURKB (aurora kinase B) expression in MI LV cardiomyocytes, including AURKB+ cardiomyocytes in metaphase, anaphase and telophase (Figure 2E through 2G; Figure S3F and S3G). Image analysis showed increased AURKB+

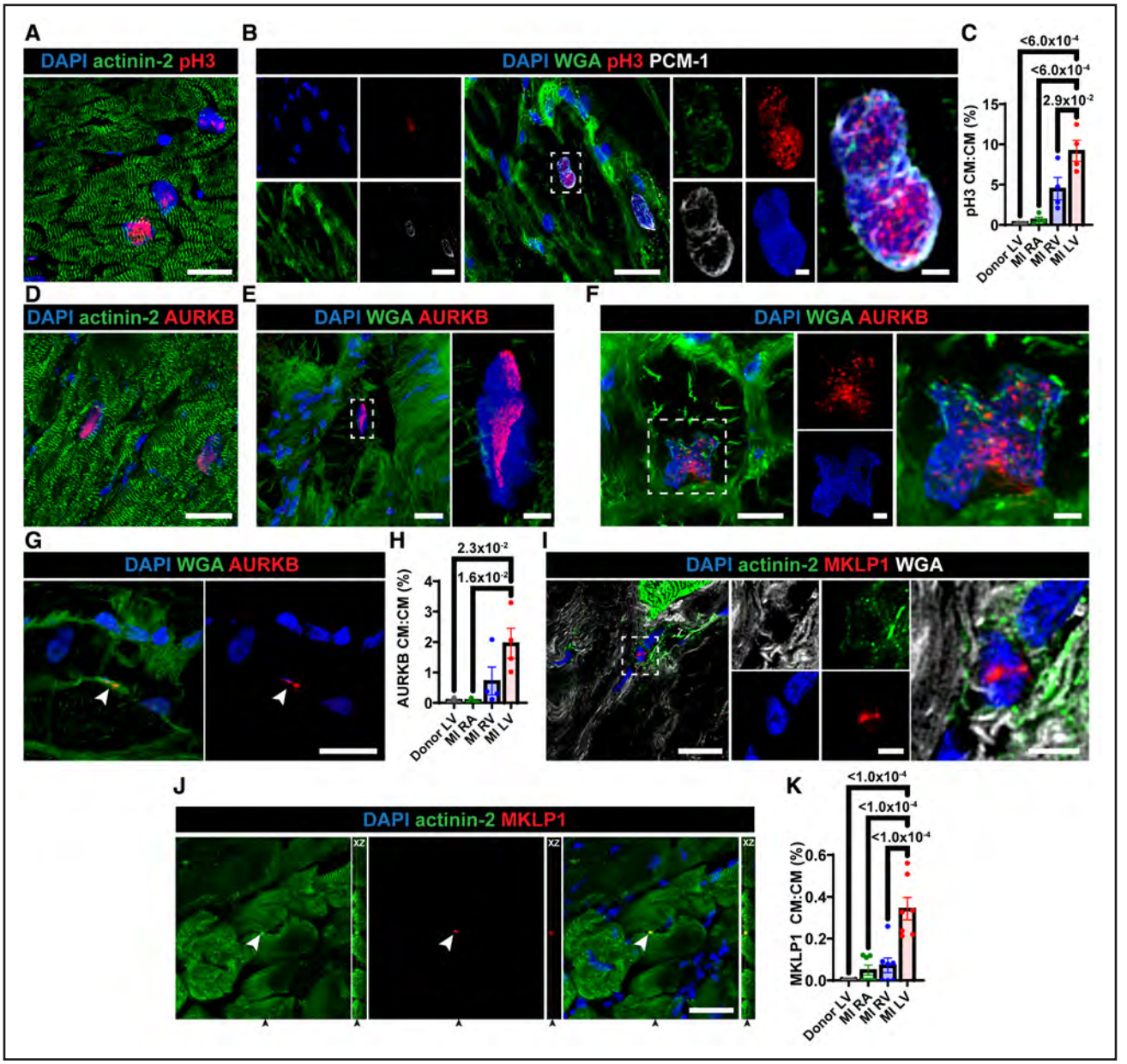

Figure 2. Human cardiomyocytes (CM) show increased mitosis following myocardial infarction (MI).
Immunohistochemistry (IHC) of infarcted human left ventricle (ischemic left ventricle [MI LV]) CM mitosis. **A**, MI LV CM (actinin-2+, green) nuclei (DAPI [4′,6-diamidino-2-phenylindole], blue) expressing mitotic marker pH3 (phospho-histone H3; red). **B**, MI LV pH3+ (red) mitotic dividing CM nuclei (perinuclear PCM-1+ [pericentriolar material 1], white) within WGA (wheat germ agglutinin)+ CM basement membrane (green). **C**, Image analysis of pH3+ CM nuclei as a proportion of all CMs (partially ischemic right ventricle [MI RV], nonischemic right atrium [MI RA], healthy nonischemic donor LV [Donor LV], n=4). **D**, MI LV CM (actinin-2+, green) nuclei (DAPI, blue) expressing mitotic marker AURKB (aurora kinase B, red) in prophase. **E** and **F**, MI LV AURKB+ (red) mitotic dividing CM nuclei (DAPI, blue) surrounded by WGA+ (green) CM basement membrane in (**E**) metaphase, and (**F**) anaphase. **G**, AURKB+ cleavage furrow between 2 CMs in cytokinesis. **H**, Image analysis of AURKB+ CM as a proportion of all CMs, n=4. **I**, MI LV dividing CMs with cytokinesis marker MKLP1 (mitotic kinesin-like protein 1) (red) expression between 2 CM nuclei. **J**, Three-dimensional z-stack of MI LV showing MKLP1+ cleavage furrow between 2 dividing CM cytoplasm. **K**, Image analysis of MKLP1+ CMs as a proportion of all CMs, n=6. Scale bars **A** through **G**=20 µm/2 µm inserts, **I** and **J**=50 µm/5 µm insert (**I**) and 50 µm XZ orthogonal view (**J**). *P* values calculated using a 1-way ANOVA test with Tukey multiple comparison test.

cardiomyocytes in MI LV, as compared with nonischemic MI RA and Donor LV controls (Figure 2H). To our knowledge, this proportion of LV mitotic cardiomyocytes (9.19% pH3$^+$ and 1.96% AURKB$^+$) has not been previously reported in adult humans.

Although cycling human cardiomyocytes are known to complete karyokinesis (nuclear division), during adulthood, they often fail to complete cytokinesis (cytoplasmic division), thus resulting in binucleated or multinucleated polyploid cells.[1] However, in an injury setting, mammalian models have shown mitotic cardiomyocytes can complete cytokinesis at the infarct border zone.[7,8,16] Using immunohistochemistry, we found instances in MI LV of cardiomyocyte nuclei splitting into 2 daughter cells, with their cytoplasm partially separated by WGA$^+$ basement membrane (Figure S3H). We also detected the cytokinesis marker MKLP1 (mitotic kinesin-like protein 1) accumulation at the cleavage furrow between newly divided cardiomyocytes (Figure 2I and 2J), providing bona fide evidence of cytokinesis.[6,17] As with pH3$^+$ cardiomyocytes and AURKB$^+$ cardiomyocytes, the proportion of MKLP1$^+$ cardiomyocytes followed a gradient of ischemia: Donor LV (0.01%) <MI RA (0.05%) <MI RV (0.07%) <MI LV (0.34%; Figure 2K). To our knowledge, only a proportion of 0.005% to 0.01% MKLP1$^+$ cardiomyocytes have previously been detected in (nonischemic) human hearts and only in adults aged <20 years.[6] Thus, our 48-year-old MI LV (ischemic) samples exhibited a proportion of MKLP1$^+$ cardiomyocytes significantly higher than previously reported in (nonischemic) human hearts, in an age range where cytokinesis has not previously been observed.[6]

Post-MI Human Heart With Increased Cardiomyocyte Mitosis Shows Increased Mononucleated Cardiomyocytes

To assess whether the increased cardiomyocyte mitosis we observed had resulted in increased binucleation (karyokinesis) or increased mononucleation (cytokinesis), we used 3-dimensional immunofluorescence[18] (Figure 3A through 3C). Using this approach with thick (50 µm) sections, we assessed the number of cardiomyocyte nuclei (DAPI$^+$ PCM$^+$) within cardiomyocyte 3-dimensional volumes (cardiomyocyte basement membranes, WGA$^+$), observing both multinucleated and dividing cardiomyocyte nuclei (Figure 3A through 3C). Similar to previous reporting that used isolated cardiomyocyte binucleation analyses, the right atrium (MI RA) had predominantly (95.74%) mononucleated cardiomyocytes,[19] whereas Donor LV controls showed 56.45% mononucleated cardiomyocytes[6] (Figure 3D). Thus, our novel method for assessing cardiomyocyte nucleation in situ agrees with published studies that require complex cardiomyocyte isolation and immunocytochemistry protocols. In contrast to nonischemic controls, both MI RV and MI LV showed increased mononucleated cardiomyocytes (77.85% and 80.94%, respectively), as compared with Donor LV (Figure 3D). This shows the increased cardiomyocyte mitosis observed earlier in our study (Figure 2; Figure S3) did not cause an increase in multinucleated cardiomyocytes via increased karyokinesis without cytokinesis, thus supporting our findings of increased cardiomyocyte cytokinesis.

Post-MI, cardiomyocytes exhibit increased DNA damage and increased nuclear polyploidization.[19] Thus, using immunohistochemistry, we assessed phospho-γH2A.X nuclear expression as a measure of DNA damage (Figure 3E and 3F). Using this approach, we confirmed that MI LV noncardiomyocyte total cell numbers increased, whereas cardiomyocyte numbers decreased post-MI, compared with Donor LV (Figure 3G and 3H). In addition, we showed that DNA damage was significantly increased in both ischemic MI LV noncardiomyocytes and MI LV cardiomyocytes, as compared with nonischemic Donor LV (Figure 3I and 3J). Next, we utilized DNA in situ hybridization to determine cardiomyocyte ploidy and showed cardiomyocyte nuclear polyploidization increased in MI LV, as compared with Donor LV (Figure 3K and 3L). These data demonstrate that increased MI LV cardiomyocyte mitosis occurred simultaneously with increased DNA damage and polyploidy.

Multiomics Shows the Post-MI Human Heart Upregulates Transcripts, Proteins and Metabolites Known to Increase Cardiomyocyte Mitosis

To further characterize the infarcted heart, we undertook a multiomics approach, utilizing transcriptomics (bulk RNA sequencing [RNAseq]; Donor LV n=7, MI RA n=2, MI RV n=5, MI LV n=5), proteomics (Donor LV n=4, MI RV n=5, MI LV n=5), and metabolomics (Donor LV n=5, MI LV n=5). Using these techniques, we compared MI LV, MI RV and MI RA to age/sex-matched healthy Donor LV samples. Expectedly, multidimensional scaling analysis of RNAseq data showed separation of nonischemic Donor LV and ischemic MI samples (Figure 4A). Repeating these comparisons without Donor LV, multidimensional scaling plots also showed separation of MI LV and MI RV that was not previously apparent (Figure S4). Differential gene expression analysis of MI LV versus Donor LV showed 1830 upregulated transcripts, including genes previously reported to induce adult cardiomyocyte mitosis: *YAP1*,[23] *IGF2* (insulin growth factor 2),[20] *AGRN* (agrin),[21] and *DCN* (decorin)[22] (Figure 4B). Among the 1036 downregulated transcripts was cell cycle inhibitor *CDKN1C* (aka *p57*; Figure 4B), which reportedly enhances adult mouse cardiomyocyte cell cycle reentry when knocked down in genetic mouse models.[24] Gene

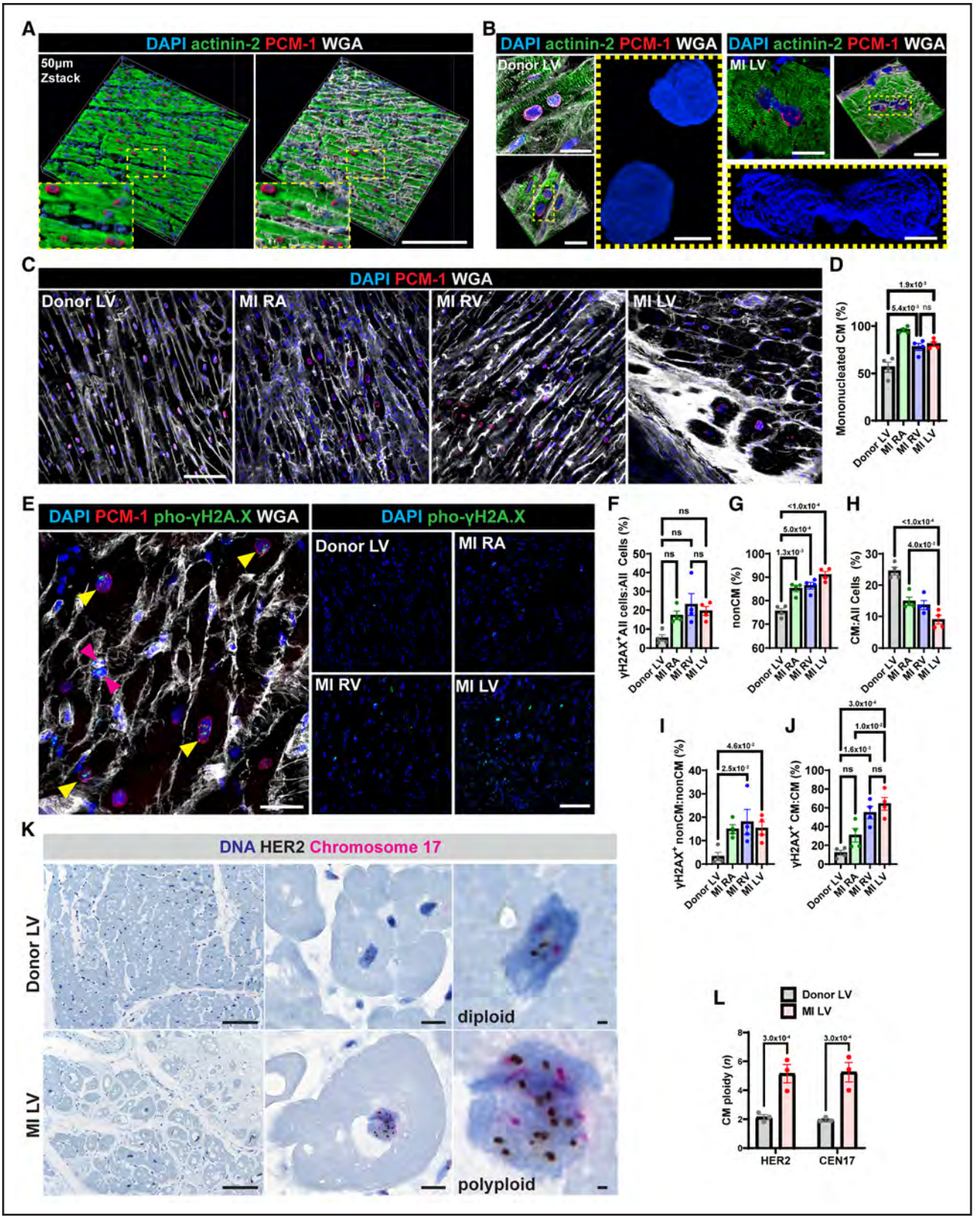

Figure 3. Postmyocardial infarction (MI) human heart with increased cardiomyocyte (CM) mitosis shows increased mononucleated CMs, DNA damage and polyploidy.

A and **B**, 50 µm 3-dimensional (3D) volume renders of MI left ventricular (LV) CM sarcomeres (actinin-2$^+$, green), CM nuclei (perinuclear PCM-1$^+$ [pericentriolar material 1], red; DAPI$^+$ [4′,6-diamidino-2-phenylindole], blue) and CM basement membranes (WGA$^+$ [wheat germ agglutinin], white). **B**, **left**, Binucleated CM in Donor LV. **Right**, CM dividing nuclei in ischemic left ventricle (MI LV), with 3D volume renders of DAPI. (*Continued*)

ontology term analysis of MI LV versus Donor LV showed upregulation of immune and ECM (extracellular matrix) pathway-related terms and downregulation of fatty acid metabolism-related terms, that is, lauric acid metabolic process and oxylipin biosynthetic process (Figure 4C). The latter is a characteristic observed in both immature cardiomyocytes and during metabolic rewiring-induced cardiac regeneration in mice.[25] Similar to postinfarct remodeling seen in rodent models, proteomics and subsequent pathway analyses of MI LV versus Donor LV showed upregulation of proteins and pathways associated with neutrophils (MPO [myeloperoxidase]. ELANE [neutrophil elastase]), monocytes/macrophages (cluster of differentiation (CD)14), fibroblasts (THY1 [thymocyte differentiation antigen 1], VIM [vimentin]), endothelial cells (VWF [von Willebrand Factor]), and elastogenesis[26] (Figure S4B; Figure S5). Notably, MI LV also showed upregulation of TGFBI (transforming growth factor beta–induced), IGF2, AGRN, and DCN proteins, which have been reported to induce cardiomyocyte mitosis in mouse models[20–22] (Figure 4D and 4E), whereas downregulated proteomics Gene Ontology terms included pathways relating to fatty acid metabolism (Figure 4F).

Recently, studies have identified multiple metabolic pathways and metabolites that can increase adult mouse cardiomyocyte mitosis post-MI, such as upregulation of the mevalonate pathway,[27] increased malonate,[28] and increased ketogenesis.[29] In addition, it has been shown that the promitotic embryonic heart switches from glucose metabolism to fatty acid oxidation postnatally and that blocking cardiomyocyte fatty acid oxidation induces cardiac regeneration in adult mice.[25] Thus, to assess whether these metabolites/pathways were altered in the post-MI human heart, we used a combination of hydrophilic interaction liquid chromatography and hydrophilic interaction liquid chromatography with an amide transition paired to tandem mass spectrometry metabolomics methods to compare MI LV versus Donor LV. Using this approach, the top upregulated metabolite in the MI LV patient (a known smoker) versus Donor LV (nonsmokers) was the nicotine metabolite cotinine[30] (Figure 4G), supporting the validity of our assay. Similar to previously mentioned rodent cardiac regeneration studies, the MI LV also showed increased mevalonate, malonate, ketone bodies (3-hydroxybutyrate and acetoacetate), ketogenic substrate HMG-CoA (β-hydroxy β-methylglutaryl-coenzyme A), short-chain ketoacid 2-oxobutanoate, and central carbon metabolite glyceraldehyde-3-phosphate (an intermediate in both glycolysis and gluconeogenesis; Figure 4G). For an understanding of the metabolic pathways affected by these changes in the MI LV, we performed an integrated metabolite-protein pathway analysis (Figure 4H). Using this approach, we saw upregulation of proteins and metabolites involved in glycolysis or glyconeogenesis (similar to what has been observed in the embryonic mouse heart[25]) and synthesis or degradation of ketone bodies (similar to mouse models of cardiac regeneration[27–29]). Together, these omics data sets show the human MI LV upregulates transcripts, proteins, metabolites and pathways that have previously been reported to induce adult cardiomyocyte regeneration in mouse MI models.[20–23,25,27–29]

Single-Nucleus RNAseq Shows Mitotic Cycling in Adult Human Cardiomyocytes Increases After MI

To further validate our findings, we performed analyses on the largest (n=191 795) independent snRNAseq human MI data set currently available[31] to identify post-MI mitotic cycling cardiomyocytes. Using unbiased clustering analysis, followed by gene set enrichment analysis for cell type–specific markers, we identified 9 distinct cell populations (Figure 5A). By using the cardiomyocyte subpopulation to compare cardiomyocyte proportions, we show an expected reduction of cardiomyocytes in the MI LV group, likely attributed to cardiomyocyte necrotic cell death after MI (Figure 5B). Next, all mitotic cycling cells were identified by enrichment for S-phase or G2/M-phase marker gene expression. As expected, MI samples showed an increased proportion of mitotic cycling cells:all cells as compared with Donor LV (Figure 5C and 5D), likely driven by post-MI increased stromal cell infiltration and mitosis. Using this same approach within the cardiomyocyte population, we identified mitotic cycling cardiomyocytes enriched for S-phase or G2/M marker expression and showed an increase in the proportion of mitotic cycling cardiomyocytes:cardiomyocyte in MI samples (Figure 5E through 5G). This independent data set provides further evidence that the number of

Figure 3 Continued. **C**, 3D immunohistochemistry (IHC) maximum intensity projections of nonischemic controls (Donor LV, nonischemic right atrium [MI RA]) and partially ischemic right ventricle (MI RV), MI LV for 3D in situ binucleation analyses. **D**, Mononucleated CMs (%) as a proportion of all CMs (n=4). **E**, IHC showing DNA damage (phosphoralated gamma-H2A histone family member X, pho-γH2A.X$^+$, green) within CM nuclei (arrowheads, yellow; perinuclear PCM-1$^+$, red; WGA$^+$ basement membrane, white) and stromal cell nuclei (arrowheads, pink). **F** through **J**, Image analysis (n=4) of (**F**) γH2A.X$^+$ DNA damage in all cells, (**G**) proportion of non-CMs nuclei (PCM-1^{neg}), (**H**) proportion of CM nuclei (PCM-1$^+$), (**I**) γH2A.X$^+$ non-CMs (PCM-1^{neg}) as a proportion of non-CMs, (**J**) γH2A.X$^+$ CMs (PCM-1$^+$) as a proportion of CMs. **K**, DNA in situ hybridization for *HER2* gene (black) and the CEN17 (centromere of chromosome 17, red) within a diploid (**top**, Donor LV) and polyploid (**bottom**, MI LV) CM. **L**, CM ploidy analysis (n=3) for HER2 (human epidermal growth factor receptor 2) and CEN17. Scale bars **A**=200 µm, **B**=20 µm/2 µm inserts, **C**=100 µm, **E**=20 µm **left**/100 µm **right**, **K**=**left** 100 µm/**middle** 10 µm/**right** 1 µm. *P* values calculated using a 1-way ANOVA test with Tukey multiple comparison test.

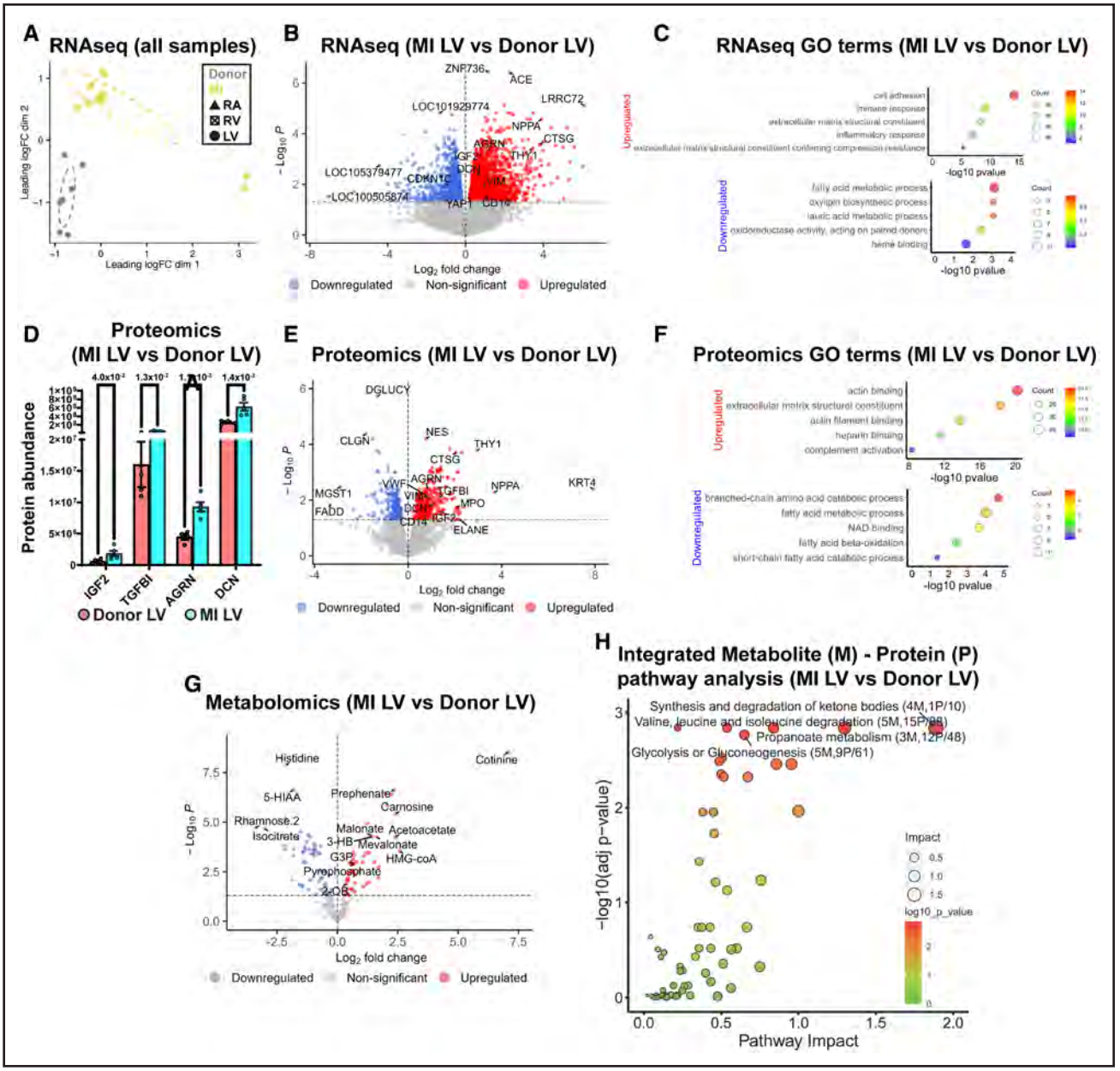

Figure 4. Multiomics shows a unique human infarcted heart upregulates transcripts, proteins and metabolites known to induce cardiomyocyte (CM) mitosis in mouse models of myocardial infarction (MI).

Transcriptomics (RNA sequencing [RNAseq]), proteomics and metabolomics of human MI samples (left ventricle: ischemic left ventricle [MI LV], right ventricle: partially ischemic right ventricle [MI RV], right atrium: nonischemic right atrium [MI RA]) and healthy age/sex-matched Donor LV samples (Donor LV). **A**, Multidimensional scaling plot of RNAseq. **B** through **H**, Omics comparisons of MI LV vs Donor LV. **B**, RNAseq volcano plot. **C**, Top 5 upregulated (red) and downregulated (blue) gene ontology (GO) terms for RNAseq. **D**, Proteomics protein abundance of proteins known to induce CM mitosis in mouse models[20–22] (unpaired multiple *t* tests with Welch correction). **E**, Proteomics volcano plot. **F**, Top 5 upregulated (red) and downregulated (blue) GO terms for proteomics. **G**, Metabolomics volcano plot. **H**, Integrated metabolite-protein metabolic pathway enrichment analysis (brackets represent number of differentially expressed metabolites (M) and proteins (P)/number of total M+P within that pathway). AGRN indicates agrin; DCN, decorin; G3P, glyceraldehyde-3-phosphate; HMG-CoA (β-hydroxy β-methylglutaryl-coenzyme A; IGF, insulin growth factor 2; LogFC, log fold change; and TGFBI, transforming growth factor beta–induced.

mitotic cardiomyocytes increases post-MI in humans. In addition, we performed snRNAseq (n=37 938) and the same bioinformatics analyses on our MI LV sample compared with an age/sex-matched Donor LV (male, 56-year-old; Figure S6). For this data set, low cell yields were achieved, likely due to infarct-related damage, and thus overinterpretation should be avoided. With this limitation, these data suggest an expected post-MI reduction in the proportion of cardiomyocytes, an increase in mitotic cycling cells, an increase in mitotic cycling cardiomyocytes, and differentially expressed genes/pathways in both MI non–mitotic cycling cardiomyocytes (aka

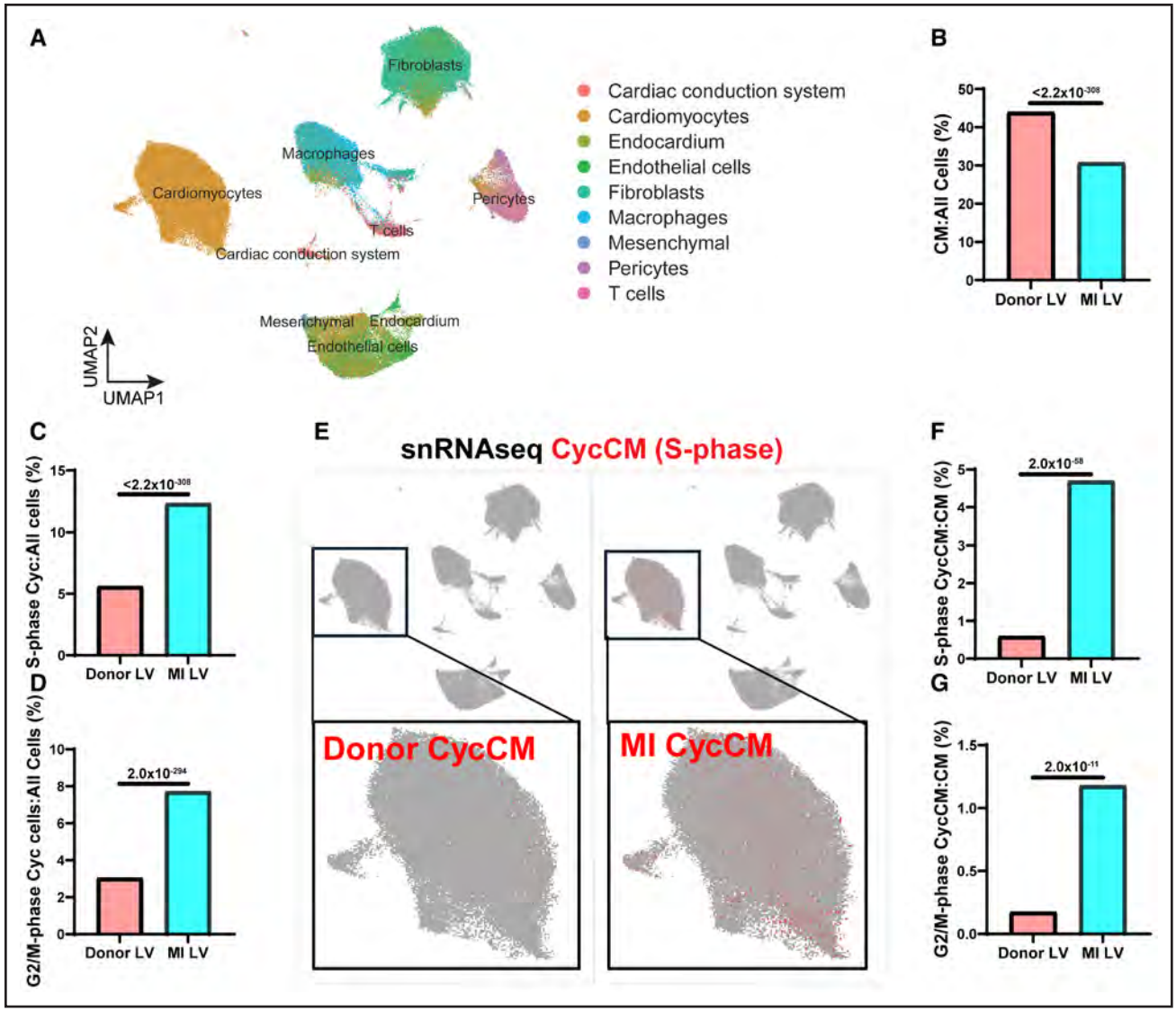

Figure 5. Single-nucleus RNA sequencing (snRNAseq) shows increased mitotic cycling cardiomyocytes (CycCM) after myocardial infarction (MI).

snRNAseq analysis of human ischemic left ventricle (MI LV) and nonischemic donor LV dataset[31] (n=191 795). **A**, Cell types identified using unbiased cluster analysis (UMAP) followed by population identification using gene set enrichment analysis (GSEA). **B**, Cardiomyocytes (CM) as a proportion of all cells. **C**, Mitotic S-phase mitotic cycling (Cyc) as a proportion of all cells. **D**, Mitotic G2/M-phase Cyc as a proportion of all cells. **E**, S-phase cycling Donor CMs (Donor CycCM, **left**, red) and MI CycCM (**right**, red) on UMAP within CM subpopulation. **F**, S-phase CycCMs as a proportion of CMs. **G**, G2/M-phase CycCMs as a proportion of all cells. *P* value calculated using Fisher exact test.

stressed cardiomyocytes[31]) and MI mitotic cycling cardiomyocytes (Figure S6).

Safe Human Biopsy Method Post-MI Shows Increased Cardiomyocyte Mitosis in the LV Peri-Infarct Border Zone

To further demonstrate the increased mitotic potential of human adult cardiomyocytes in response to post-MI ischemia, we developed a safe method to obtain LV biopsies from patients (>20yo) undergoing CABG surgery after a recent acute MI (Figure 6A; Supplemental Material for detailed methods and Table S1 for clinical characteristics). A time interval of 7 to 14 days post-MI for LV biopsy collection was chosen to capture the window of cardiomyocyte mitosis. To ensure patient safety, biopsies were collected in <5 minutes under direct visualization (thoracotomy) to identify infarct location and to enable quick resolution of any potential bleeding complications that could occur (although we observed no bleeding complications in this study). Furthermore, only senior experienced cardiothoracic surgeons performed this biopsy technique. Using these approaches, no surgeries amounted to any clinical complications or adverse events, demonstrating the safety of our technique.

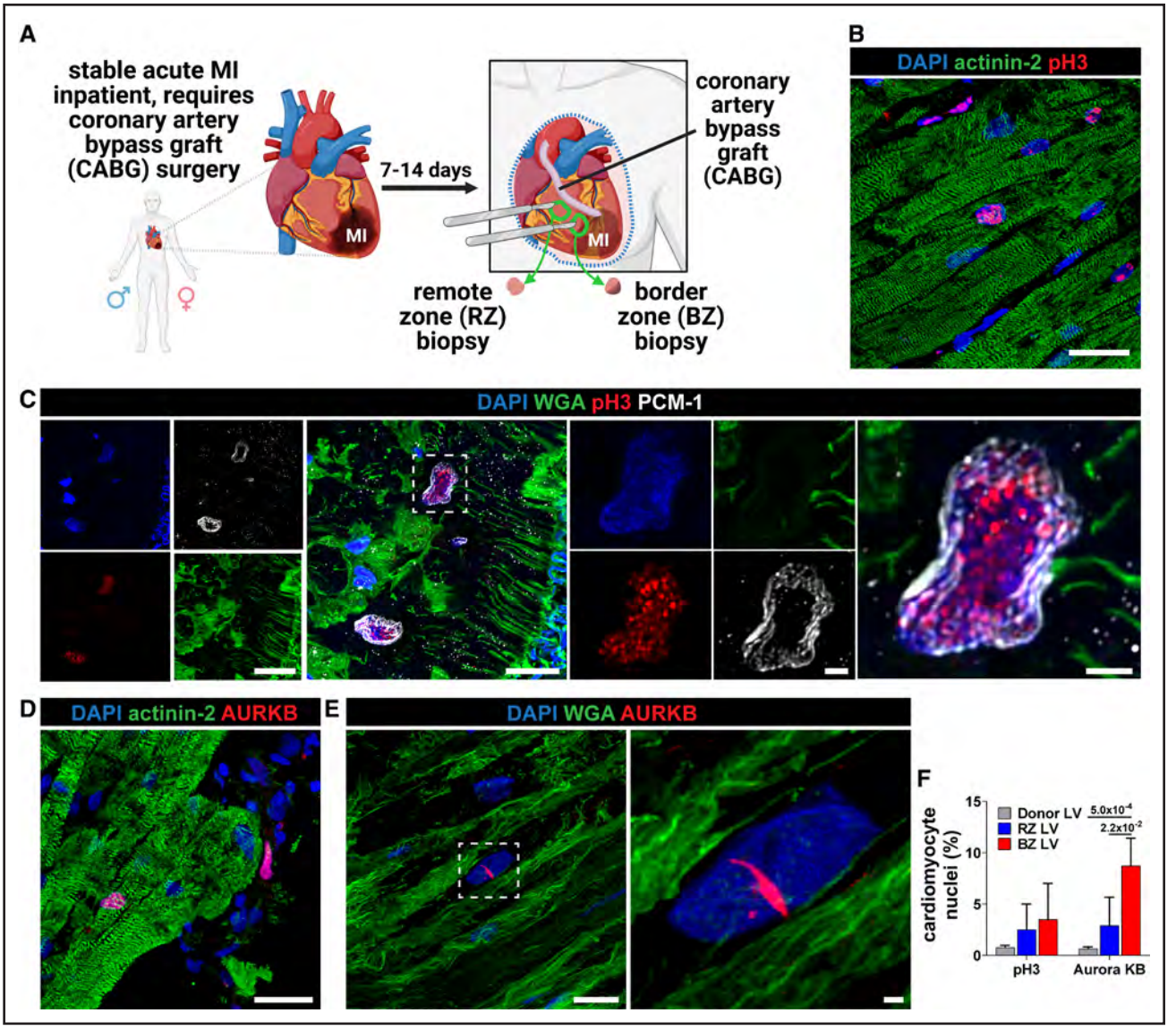

Figure 6. A novel method to safely obtain left ventricle (LV) biopsies from patients with acute myocardial infarction (MI) undergoing coronary artery bypass graft (CABG) surgery shows increased cardiomyocyte (CM) mitosis in the peri-ischemic infarct border zone left ventricle zone (BZ LV).

A, Schematic of post-MI CABG protocol to collect nonischemic healthy remote zone (RZ LV) and peri-ischemic infarct border zone (BZ LV) biopsies. **B** through **E**, Immunohistochemistry (IHC) of mitotic CMs in BZ LV. **B**, Mitotic pH3$^+$ (phospho-histone H3$^+$, red) nuclei (DAPI$^+$ [4′,6-diamidino-2-phenylindole]) within CM sarcomeres (actinin-2$^+$, green). **C**, Mitotic pH3$^+$ (red) CM nuclei (perinuclear PCM-1$^+$ [pericentriolar material 1], white; DAPI$^+$, blue) within CM basement membrane/t-tubules (WGA$^+$ [wheat germ agglutinin], green). **D**, Mitotic AURKB$^+$ (aurora kinase B, red, **left**) nuclei (DAPI$^+$) within CM sarcomeres (actinin-2$^+$, green). **E**, Mitotic AURKB$^+$ (red) CM nuclei within CM basement membrane/t-tubules (WGA$^+$, green). **F**, IHC analysis of pH3$^+$ CM and AURKB$^+$ CM in healthy nonischemic Donor LV, nonischemic RZ LV and peri-infarct BZ LV (BZ LV n=5, RZ LV n=5, error bars=SEM, *P* values calculated using a 1-way ANOVA test with Tukey multiple comparison test). Scale bars: **B**=50 µm, **C**=**left** 20 µm/**right** 2 µm, **D**=50 µm, **E**=**left** 20 µm/**right** 2 µm.

Using our method, LV myocardial biopsies were taken from the peri-ischemic border zone (BZ LV hereafter, n=6) and an area of healthy myocardium distal to the infarct, aka remote zone (LV RZ hereafter, n=6; Figure 6A). This approach closely approximates the post-MI mouse cardiac regeneration model, whereby BZ LV and RZ LV samples are typically analyzed.[7,8] As there were no clinical complications throughout the study, we propose this model to be used in future to further investigate early MI remodeling and cardiac regeneration using fresh human myocardium infarct biopsies.

To assess whether mitotic cardiomyocytes could also be identified in LV epicardial biopsies from patients with MI, we performed immunohistochemistry to analyze expression of mitotic markers pH3 and AURKB. Compared with Donor LV, both RZ LV and BZ LV biopsies showed a nonsignificant increase in pH3$^+$ (0.77% Donor LV, 2.50% RZ LV, 3.50% BZ LV) and significantly

increased AURKB+ (0.65% Donor LV, 2.90% RZ LV, 8.71% BZ LV) mitotic cardiomyocytes (Figure 6B through 6F; Figure S7A and S7B), albeit lower than observed in earlier MI LV analyses (Figure 2). Similar to earlier MI LV samples, cardiomyocyte mitosis approximately correlated with each region's degree of ischemia: Donor LV<RZ LV<BZ LV (Figure 6f). We also found one instance of 2 cardiomyocytes in late cytokinesis (MKLP1+ cleavage furrow) in our BZ LV samples (Figure S7C). These results further demonstrate that adult human cardiomyocytes increase their mitotic potential post-MI and provide a human cardiac infarct biopsy model for future studies.

DISCUSSION

Pivotal studies have shown that adult human cardiomyocytes undergo mitosis at low levels in normal development.[6,32,33] However, evidence of the increased cardiomyocyte mitosis previously observed after MI injury in rodent models[7,8] has not been shown in adult humans. This is relevant given that MI is one of the leading causes of death worldwide. In this study, we demonstrated that human adult cardiomyocytes increase both mitosis and cytokinesis in response to MI. We also characterized the ischemic environment that promoted this intrinsic cardiomyocyte cell division, identifying transcripts, proteins and metabolites previously shown to induce cardiomyocyte mitosis in rodent studies.[20–23,25,27–29] Using independent snRNAseq analysis, we also confirmed that adult human cardiomyocytes show increased mitosis in response to ischemia. Finally, we developed a novel method to obtain fresh human LV infarct biopsies from patients with MI and provided further evidence of increased adult cardiomyocyte mitosis after injury.

To the best of our knowledge, there are only 2 human studies (1 of which has been placed under expression of concern by *The New England Journal of Medicine*) that examined changes in human cardiomyocyte mitosis at the MI BZ.[34,35] Specifically, they showed a relative increase in BZ Ki-67+ cardiomyocytes post-MI. Two significant limitations of their approach were the use of Ki-67, a marker present at all stages of the cell cycle (G1, S, G2, and M-phase[36]), and the use of samples obtained postmortem, which are subject to degradation in the histological architecture of the myocardium. In contrast, we identified mitotic cardiomyocytes using pH3+ and AURKB+ markers that peak in expression during G2/M phases,[36,37] using premortem samples. We therefore provided evidence of cardiomyocytes in late-stage mitosis, likely undergoing karyokinesis, using non-postmortem samples that were collected within 15 minutes of harvest from the living. However, karyokinesis does not imply subsequent cytokinesis, particularly in the human heart, which is notorious for increasing cardiomyocyte ploidy (eg, to 16*n*) and binucleation in response to physiological stresses.[4] Therefore, to show new cardiomyocyte formation after MI, we provided evidence of cytokinesis using MKLP1 localization between newly divided cardiomyocytes, together with an increased proportion of mononucleated cardiomyocytes. This strategy was previously used by Mollova et al,[6] who showed cardiomyocytes cease to undergo cytokinesis in healthy humans >20 years old. Within this context, our findings in an older infarcted 48-year-old LV demonstrated MI enhanced cardiomyocyte cell division in a previously unreported (healthy) age at hitherto undetected levels. In addition, a recent study by the Bergmann laboratory supporting our findings has also demonstrated that human diseased hearts can intrinsically increase cardiomyocyte mitosis, albeit in a different context of mechanical unloading via LV assist device in patients with end-stage heart failure.[38]

Unlike humans, increased adult rodent cardiomyocyte mitosis post-MI has been documented for over 2 decades.[7,8] For instance, Senyo et al[7] previously showed 23.0% of BZ LV cardiomyocytes undergo new DNA synthesis 8 weeks post-MI versus 1.1% in shams, whereas 3.2% cardiomyocytes undergo cell division. This aforementioned rodent study and our human studies both demonstrate increased adult cardiomyocyte mitosis post-MI; however, there are differences in terms of the percentage of mitotic cardiomyocytes. Although species (human versus mouse) may account for these differences, there are also considerable differences in experimental models and designs, that is, 5 days versus 8 weeks post-MI, pathological MI versus surgically induced MI, and immunohistochemistry versus multi-isotope imaging mass spectrometry analyses. Regardless, the potential translational implications of our human findings are notable. For example, as we have shown, human adult cardiomyocytes hold increased mitotic potential post-MI; therapies could be developed to amplify cardiomyocyte mitosis to improve cardiac function via cardiac regeneration. Importantly, many groups are already developing such therapies in animal models[21,25,28] with potentially life-changing clinical implications for heart failure patients.

Studies investigating adult human cardiomyocyte mitosis are uncommon due to the ethical and safety restrictions for collecting live cardiac tissue and labelling cells in vivo. Of these limited studies, Bergmann et al,[33] also investigated adult human RV cardiomyocyte renewal, using healthy noninfarcted hearts labelled with ^{14}C during the Cold War era, finding no significant difference between RV cardiomyocyte versus LV cardiomyocyte renewal rates (<1%/y). In contrast, our findings in infarcted human myocardium showed cardiac chamber-specific differences in cardiomyocyte mitosis, which approximately correlated with increasing ischemia, that is, Donor LV < MI RA<MI RV<MI LV (note the MI RV was subtended by the left anterior descending coronary artery and showed partial ischemia and scar formation). This supports the hypothesis that either ischemia itself or the infarcted microenvironment (eg, cell signaling/ECM

composition/metabolic rewiring) is driving the increased cardiomyocyte mitosis observed in ischemic over non-ischemic chambers post-MI.

Historically, the failing heart was once regarded as an engine out of fuel, defined by its decrease in energy metabolism.[39] Although this paradigm has shifted in recent years,[40] myocardial energetics remains an essential tool used to deepen our understanding of heart failure. Recent studies have investigated the relationship between metabolite usage and cardiomyocyte mitosis,[27–29] whereas others have investigated the cardiomyocyte metabolic switch, that is, from the glycolytic promitotic embryonic environment, to the predominantly fatty acid oxidation within the postnatal heart.[25,27–29] Together, these groups have identified key metabolic pathways that can induce cardiomyocyte mitosis, such as the mevalonate pathway, malonate inhibition of succinate dehydrogenase, increased ketogenesis and blocking fatty acid oxidation. Specifically, the mevalonate pathway was identified as promitotic via an unbiased screening of small molecule compounds within human embryonic stem cell–derived cardiomyocytes,[27] whereas malonate, ketogenesis, and blocking fatty acid oxidation were specifically targeted using mouse models.[25,28,29] Within our infarcted human samples, all these pathways were similarly affected: mevalonate, malonate, ketogenesis, and glycolysis were upregulated, whereas fatty acid metabolism was reduced. Although it should be noted that previous cardiac regeneration rodent studies therapeutically increased transcript/protein/metabolite levels above pathophysiological levels to induce cardiac regeneration. Therefore, their pathophysiological increase in our human study during infarct remodeling cannot be explicitly linked to the observed increase in cardiomyocyte mitosis without further mechanistic studies. Although the potency of each metabolite to induce cardiomyocyte mitosis is unknown, the upregulation of multiple ketogenic metabolites and their position as the most significant/impactful upregulated pathway in our integrated metabolite-protein analysis may highlight the importance of ketogenesis in the promitotic ischemic setting. However, it should be noted that our metabolomic approach did not include the detection of metabolites downstream of mevalonate, that is, mevalonate-5-phosphate, mevalonate pyrophosphate, isopentyl pyrophosphate, and dimethylallyl pyrophosphate. Future studies should, therefore, include additional analysis of these metabolites to determine the full effect of ischemia on the promitotic mevalonate pathway in human samples.[7,8]

One limitation of our study is the sample size, which is inherent given the relative infrequency of organ donation. Moreover, today, nearly all truly healthy donor hearts viable for transplant are successfully transplanted into heart failure recipients, due to advances in transplant management and accessibility to transplant centers. Premortem human heart tissue is, therefore, precious, with both MI (non–end-stage heart failure) and donor hearts rarely available for research. For the unique premortem infarcted heart used in our study, the after prerequisites were required: (1) the next of kin consent had been undertaken as part of a national donor program, (2) the patient suffered an out of hospital cardiac arrest secondary to MI via full left anterior descending coronary artery occlusion but did not display neurological activity compatible with life while on life support for 5 days, (3) the next of kin gave consent for organ donation for research (given the heart could not be transplanted), and (4) the whole heart was collected premortem (not postmortem). As these simultaneous events were required to acquire the samples, it is unlikely that such a premortem ischemic heart will be available again.

To provide a tool to study cardiomyocyte mitosis in an organotypic model that does not require rare samples, we developed our novel MI CABG biopsy method. This allowed us to acquire fresh human border zone periischemic infarct myocardium, along with remote zone healthy control tissue from patients with MI. Although this protocol allows researchers to collect and study live human infarct tissue, it does have limitations. For instance, due to ethical and patient safety concerns (eg, postoperative bleeding) when surgically removing myocardium from below the epicardium, only small (1–5 mm^3) biopsies could be collected. Although tissue harvesting was done under direct visualization via thoracotomy (during CABG), allowing potential bleeding to be sutured immediately, these safety concerns still limited the amount of tissue collected. However, an advantage of live biopsy collections, is that future experiments could include live tissue culture with 5-ethynyl-2'-deoxyuridine, a nucleoside analog of thymidine that is incorporated into newly synthesized DNA. Optimization of this approach would allow live visualization and tracing of dividing human cardiomyocytes in an organotypic in vitro model. For clinical applications, this model could potentially be utilized as a low-throughput therapeutic testing platform, to complement higher throughput models, such as induced pluripotent stem cell–derived cardiomyocytes.

Similar to the infarcted heart, early normal mammalian cardiac development (and regeneration) occurs in a low-oxygen environment,[41] with altered cardiac ECM expression.[21,22,42] Our data support these observations, showing global (bulk RNAseq and proteomics) ECM modulation. This included ECM transcripts and proteins known to be upregulated during embryonic development and known to induce cardiomyocyte mitosis in mouse models (eg, AGRN, TGFBI, DCN[21,22,42]). Although these findings were the result of comprehensive characterization of a unique ischemic heart, it is unlikely that similar tissue will be collected again. As such, we suggest our human LV heart failure biopsy method as a highly suitable candidate model for future studies.

In conclusion, our study shows that the infarcted human heart increases cardiomyocyte mitosis in response to ischemia. Although this intrinsic ability to increase mitosis is not sufficient to replace the cardiomyocytes lost after MI, studies aiming to therapeutically enhance cardiomyocyte proliferation to reverse heart failure are underway.[20,27,28] Thus, developing means to enhance this intrinsic cardiomyocyte mitotic potential could lead to novel therapeutics for cardiac injury and heart failure.

ARTICLE INFORMATION

Received September 08, 2025; revision received October 31, 2025; accepted November 17, 2025.

Affiliations

School of Medical Sciences, Faculty of Medicine and Health (R.D.H., J.W., C.M., L.S., D.H., E.S., X.W., L.N., L.C., A.L.F., M.L., S.L.), The Charles Perkins Centre (R.D.H., J.W., C.M., L.S., D.H., A.L.F., M.L., J.F.O., P.B., S.L.), and Sydney Medical School (F.N.R., C.H., A.G., J.J.H.C., P.B.), University of Sydney, Sydney, New South Wales, Australia. Centre for Heart Failure and Diseases of the Aorta, The Baird Institute, Sydney, New South Wales, Australia (R.D.H., C.M., L.S., J.F.O., P.B., S.L.). Institute for Molecular Bioscience, University of Queensland, St Lucia, Queensland, Australia (W.J.S., N.J.P.). Walter and Eliza Hall Institute of Medical Research, Melbourne, Victoria, Australia (M. Li). Tissue Pathology and Diagnostic Oncology, NSW Health Pathology (J.D., T.L., G.T., W.C.), Department of Cardiothoracic Surgery (J.E., P.B.) and Department of Cardiology (J.F.O., S.L.), Royal Prince Alfred Hospital, Sydney, New South Wales, Australia. Centre for Heart Research, Westmead Institute for Medical Research, Sydney, New South Wales, Australia (F.N.R., J.J.H.C.). Liver Injury and Cancer Program, Centenary Institute, Sydney, New South Wales, Australia (A.L.F.). Department of Cardiology, Westmead Hospital, Sydney, New South Wales, Australia (J.J.H.C.). Now with ithree Institute, Faculty of Science, University of Technology Sydney, New South Wales, Australia (L.C.). Department of Cardiothoracic Surgery and Transplantation, Fiona Stanley Hospital, Murdoch, Western Australia, Australia (J.E.). University of Western Australia, Crawley, Western Australia, Australia (J.E.)

Acknowledgments

The authors thank the patients and staff of Royal Prince Alfred Hospital and St. Vincent's Hospital, Sydney, and we thank the Australian Red Cross Blood Service. The authors acknowledge the Children's Medical Research Institute (CMRI) Single Cell Analytics, Advanced Microscopy Center, and the Australian Cancer Research Foundation Telomere Analysis Center for supporting this work. The authors acknowledge the technical and scientific assistance of Sydney Microscopy & Microanalysis, the University of Sydney node of Microscopy Australia. The authors acknowledge the Sydney Cytometry Core Research Facility, a joint initiative of Centenary Institute and the University of Sydney, for assistance with imaging mass cytometry.

Author Contributions

R.D. Hume conducted experiments, contributed to experimental design and wrote the manuscript; J. Warwick conducted experiments and wrote the manuscript; W.J. Shim, M. Li, and E. Slaughter conducted bioinformatic analysis; C. Malecki, D. Harney, X. Wang, L. Nguyen, L. Cole, and M. Li conducted experiments; J. Edelman, F. Rashid, A.L. Ferguson, J.J.H. Chong, N. Palpant, and J. O'Sullivan contributed to experimental design; C. Houlahan and A. Gao performed analyses; P. Bannon contributed to experimental design and conducted experiments; S. Lal conceived the project, designed experiments, conducted experiments and wrote the manuscript.

Sources of Funding

This work was supported by a grant from the R.T. Hall Trust and the support of the Baird Institute for Applied Heart and Lung Research. N.J. Palpant acknowledges the following grants supporting this work: Heart Foundation grant 106721 and Medical Research Future Fund (MRFF) grant APP2007625.

Disclosures

None.

Supplemental Material

Figures S1-S8
Supplemental Methods
References 43-59
Table S1
Figures S1–S8
Major Resources Table
Data Code Availability

REFERENCES

1. Laflamme MA, Murry CE. Heart regeneration. *Nature*. 2011;473:326–335. doi: 10.1038/nature10147
2. Senyo SE, Lee RT, Kühn B. Cardiac regeneration based on mechanisms of cardiomyocyte proliferation and differentiation. *Stem Cell Res*. 2014;13:532–541. doi: 10.1016/j.scr.2014.09.003
3. Ponikowski P, Voors AA, Anker SD, Bueno H, Cleland JGF, Coats AJS, Falk V, González-Juanatey JR, Harjola VP, Jankowska EA, et al; ESC Scientific Document Group. 2016 ESC guidelines for the diagnosis and treatment of acute and chronic heart failure: the Task Force for the diagnosis and treatment of acute and chronic heart failure of the European Society of Cardiology (ESC) developed with the special contribution of the Heart Failure Association (HFA) of the ESC. *Eur Heart J*. 2016;37:2129–2200. doi: 10.1093/eurheartj/ehw128
4. Boström P, Frisén J. New cells in old hearts. *N Engl J Med*. 2013;368:1358–1360. doi: 10.1056/NEJMcibr1300157
5. Porrello ER, Mahmoud AI, Simpson E, Hill JA, Richardson JA, Olson EN, Sadek HA. Transient regenerative potential of the neonatal mouse heart. *Science*. 2011;331:1078–1080. doi: 10.1126/science.1200708
6. Mollova M, Bersell K, Walsh S, Savla J, Das LT, Park SY, Silberstein LE, Dos Remedios CG, Graham D, Colan S, et al. Cardiomyocyte proliferation contributes to heart growth in young humans. *Proc Natl Acad Sci USA*. 2013;110:1446–1451. doi: 10.1073/pnas.1214608110
7. Senyo SE, Steinhauser ML, Pizzimenti CL, Yang VK, Cai L, Wang M, Wu TD, Guerquin-Kern JL, Lechene CP, Lee RT. Mammalian heart renewal by pre-existing cardiomyocytes. *Nature*. 2013;493:433–436. doi: 10.1038/NATURE11682
8. Wang WE, Li L, Xia X, Fu W, Liao Q, Lan C, Yang D, Chen H, Yue R, Zeng C, et al. Dedifferentiation, proliferation, and redifferentiation of adult mammalian cardiomyocytes after ischemic injury. *Circulation*. 2017;136:834–848. doi: 10.1161/CIRCULATIONAHA.116.024307
9. Chien KR, Frisén J, Fritsche-Danielson R, Melton DA, Murry CE, Weissman IL. Regenerating the field of cardiovascular cell therapy. *Nat Biotechnol*. 2019;37:232–237. doi: 10.1038/s41587-019-0042-1
10. Lal S, Li A, Allen D, Allen PD, Bannon P, Cartmill T, Cooke R, Farnsworth A, Keogh A, dos Remedios C. Best practice biobanking of human heart tissue. *Biophys Rev*. 2015;7:399–406. doi: 10.1007/s12551-015-0182-6
11. Hume RD, Deshmukh T, Doan T, Shim WJ, Kanagalingam S, Tallapragada V, Rashid F, Marcuello M, Blessing D, Selvakumar D, et al. PDGF-AB reduces myofibroblast differentiation without increasing proliferation after myocardial infarction. *JACC Basic Transl Sci*. 2023;8:658–674. doi: 10.1016/j.jacbts.2022.11.006
12. Harney DJ, Hutchison AT, Su Z, Hatchwell L, Heilbronn LK, Hocking S, James DE, Larance M. Small-protein enrichment assay enables the rapid, unbiased analysis of over 100 low abundance factors from human plasma. *Mol Cell Proteomics*. 2019;18:1899–1915. doi: 10.1074/mcp.TIR119.001562
13. Koay YC, Stanton K, Kienzle V, Li M, Yang J, Celermajer DS, O'Sullivan JF. Effect of chronic exercise in healthy young male adults: a metabolomic analysis. *Cardiovasc Res*. 2021;117:613–622. doi: 10.1093/cvr/cvaa051
14. O'Sullivan JF, Morningstar JE, Yang Q, Zheng B, Gao Y, Jeanfavre S, Scott J, Fernandez C, Zheng H, O'Connor S, et al. Dimethylguanidino valeric acid is a marker of liver fat and predicts diabetes. *J Clin Invest*. 2017;127:4394–4402. doi: 10.1172/JCI95995
15. Hume RD, Chong JJH. The cardiac injury immune response as a target for regenerative and cellular therapies. *Clin Ther*. 2020;42:1923–1943. doi: 10.1016/j.clinthera.2020.09.006
16. Nishiyama C, Saito Y, Sakaguchi A, Kaneko M, Kiyonari H, Xu Y, Arima Y, Uosaki H, Kimura W. Prolonged myocardial regenerative capacity in neonatal opossum. *Circulation*. 2022;146:125–139. doi: 10.1161/CIRCULATIONAHA.121.055269
17. Capalbo L, Bassi ZI, Geymonat M, Todesca S, Copoiu L, Enright AJ, Callaini G, Riparbelli MG, Yu L, Choudhary JS, et al. The midbody interactome reveals unexpected roles for PP1 phosphatases in cytokinesis. *Nat Commun*. 2019;10:4513. doi: 10.1038/s41467-019-12507-9

18. Taper M, Carrington G, Peckham M, Lal S, Hume RD. A comparison of fixation and immunofluorescence protocols for successful reproducibility and improved signal in human left ventricle cardiac tissue. *J Microsc*. 2024;296:34–47. doi: 10.1111/jmi.13336
19. Derks W, Bergmann O. Polyploidy in cardiomyocytes: roadblock to heart regeneration? *Circ Res*. 2020;126:552–565. doi: 10.1161/CIRCRESAHA.119.315408
20. Shen H, Gan P, Wang K, Darehzereshki A, Wang K, Kumar SR, Lien CL, Patterson M, Tao G, Sucov HM. Mononuclear diploid cardiomyocytes support neonatal mouse heart regeneration in response to paracrine IGF2 signaling. *Elife*. 2020;9:e53071. doi: 10.7554/ELIFE.53071
21. Bassat E, Mutlak YE, Genzelinakh A, Shadrin IY, Baruch Umansky K, Yifa O, Kain D, Rajchman D, Leach J, Riabov Bassat D, et al. The extracellular matrix protein agrin promotes heart regeneration in mice. *Nature*. 2017;547:179–184. doi: 10.1038/nature22978
22. Gáspár R, Gömöri K, Kiss B, Szántai A, Pálóczi J, Varga ZV, Pipis J, Váradi B, Ágg B, Csont T, et al. Decorin protects cardiac myocytes against simulated ischemia/reperfusion injury. *Molecules*. 2020;25:3426. doi: 10.3390/molecules25153426
23. Xin M, Kim Y, Sutherland LB, Murakami M, Qi X, McAnally J, Porrello ER, Mahmoud AI, Tan W, Shelton JM, et al. Hippo pathway effector Yap promotes cardiac regeneration. *Proc Natl Acad Sci USA*. 2013;110:13839–13844. doi: 10.1073/pnas.1313192110
24. Di Stefano V, Giacca M, Capogrossi MC, Crescenzi M, Martelli F. Knockdown of cyclin-dependent kinase inhibitors induces cardiomyocyte re-entry in the cell cycle. *J Biol Chem*. 2011;286:8644–8654. doi: 10.1074/jbc.M110.184549
25. Li X, Wu F, Günther S, Looso M, Kuenne C, Zhang T, Wiesnet M, Klatt S, Zukunft S, Fleming I, et al. Inhibition of fatty acid oxidation enables heart regeneration in adult mice. *Nature*. 2023;622:619–626. doi: 10.1038/s41586-023-06585-5
26. Hume RD, Kanagalingam S, Deshmukh T, Chen S, Mithieux SM, Rashid FN, Roohani I, Lu J, Doan T, Graham D, et al. Tropoelastin improves post-infarct cardiac function. *Circ Res*. 2023;132:72–86. doi: 10.1161/CIRCRESAHA.122.321123
27. Mills RJ, Parker BL, Quaife-Ryan GA, Voges HK, Needham EJ, Bornot A, Ding M, Andersson H, Polla M, Elliott DA, et al. Drug screening in human PSC-cardiac organoids identifies pro-proliferative compounds acting via the mevalonate pathway. *Cell Stem Cell*. 2019;24:895.e6–907.e6. doi: 10.1016/j.stem.2019.03.009
28. Bae J, Salamon RJ, Brandt EB, Paltzer WG, Zhang Z, Britt EC, Hacker TA, Fan J, Mahmoud AI. Malonate promotes adult cardiomyocyte proliferation and heart regeneration. *Circulation*. 2021;143:1973–1986. doi: 10.1161/CIRCULATIONAHA.120.049952
29. Cheng YY, Gregorich Z, Prajnamitra RP, Lundy DJ, Ma TY, Huang YH, Lee YC, Ruan SC, Lin JH, Lin PJ, et al. Metabolic changes associated with cardiomyocyte dedifferentiation enable adult mammalian cardiac regeneration. *Circulation*. 2022;146:1950–1967. doi: 10.1161/CIRCULATIONAHA.122.061960
30. Tan X, Vrana K, Ding ZM. Cotinine: pharmacologically active metabolite of nicotine and neural mechanisms for its actions. *Front Behav Neurosci*. 2021;15:758252. doi: 10.3389/fnbeh.2021.758252
31. Kuppe C, Ramirez Flores RO, Li Z, Hayat S, Levinson RT, Liao X, Hannani MT, Tanevski J, Wünnemann F, Nagai JS, et al. Spatial multi-omic map of human myocardial infarction. *Nature*. 2022;608:766–777. doi: 10.1038/s41586-022-05060-x
32. Bergmann O, Bhardwaj RD, Bernard S, Zdunek S, Barnabé-Heide F, Walsh S, Zupicich J, Alkass K, Buchholz BA, Druid H, et al. Evidence for cardiomyocyte renewal in humans. *Science*. 2009;324:98–102. doi: 10.1126/SCIENCE.1164680
33. Bergmann O, Zdunek S, Felker A, Salehpour M, Alkass K, Bernard S, Sjostrom SL, Szewczykowska M, Jackowska T, Dos Remedios C, et al. Dynamics of cell generation and turnover in the human heart. *Cell*. 2015;161:1566–1575. doi: 10.1016/j.cell.2015.05.026
34. Meckert PC, Rivello HG, Vigliano C, González P, Favaloro R, Laguens R. Endomitosis and polyploidization of myocardial cells in the periphery of human acute myocardial infarction. *Cardiovasc Res*. 2005;67:116–123. doi: 10.1016/j.cardiores.2005.02.017
35. Beltrami AP, Urbanek K, Kajstura J, Yan SM, Finato N, Bussani R, Nadal-Ginard B, Silvestri F, Leri A, Beltrami CA, et al. Evidence that human cardiac myocytes divide after myocardial infarction. *N Engl J Med*. 2001;344:1750–1757. doi: 10.1056/nejm200106073442303
36. Ramani P, Taylor S, Miller E, Sowa-Avugrah E, May MT. High phosphohistone H3 expression correlates with adverse clinical, biological, and pathological factors in neuroblastomas. *J Histochem Cytochem*. 2015;63:397–407. doi: 10.1369/0022155415576966
37. Basant A, Lekomtsev S, Tse YC, Zhang D, Longhini KM, Petronczki M, Glotzer M. Aurora B kinase promotes cytokinesis by inducing centralspindlin oligomers that associate with the plasma membrane. *Dev Cell*. 2015;33:204–215. doi: 10.1016/j.devcel.2015.03.015
38. Derks W, Rode J, Collin S, Rost F, Heinke P, Hariharan A, Pickel L, Simonova I, Lázár E, Graham E, et al. A latent cardiomyocyte regeneration potential in human heart disease. *Circulation*. 2025;151:245–256. doi: 10.1161/CIRCULATIONAHA.123.067156
39. Neubauer S. The failing heart--an engine out of fuel. *N Engl J Med*. 2007;356:1140–1151. doi: 10.1056/NEJMra063052
40. Ritterhoff J, Tian R. Metabolic mechanisms in physiological and pathological cardiac hypertrophy: new paradigms and challenges. *Nat Rev Cardiol*. 2023;20:812–829. doi: 10.1038/s41569-023-00887-x
41. Dunwoodie SL. The role of hypoxia in development of the Mammalian embryo. *Dev Cell*. 2009;17:755–773. doi: 10.1016/j.devcel.2009.11.008
42. Kühn B, del Monte F, Hajjar RJ, Chang YS, Lebeche D, Arab S, Keating MT. Periostin induces proliferation of differentiated cardiomyocytes and promotes cardiac repair. *Nat Med*. 2007;13:962–969. doi: 10.1038/nm1619
43. Thavapalachandran S, Grieve SM, Hume RD, Le TYL, Raguram K, Hudson JE, Pouliopoulos J, Figtree GA, Dye RP, Barry AM, et al. Platelet-derived growth factor-AB improves scar mechanics and vascularity after myocardial infarction. *Sci Transl Med*. 2020;12:eaay2140. doi: 10.1126/scitranslmed.aay2140
44. Ashhurst TM, Marsh-Wakefield F, Putri GH, Spiteri AG, Shinko D, Read MN, Smith AL, King NJC. Integration, exploration, and analysis of high-dimensional single-cell cytometry data using Spectre. *Cytometry A*. 2022;101:237–253. doi: 10.1002/cyto.a.24350
45. Liao Y, Smyth GK, Shi W. The R package Rsubread is easier, faster, cheaper and better for alignment and quantification of RNA sequencing reads. *Nucleic Acids Res*. 2019;47:e47–e47. doi: 10.1093/nar/gkz114
46. Robinson MD, McCarthy DJ, Smyth GK. edgeR: a bioconductor package for differential expression analysis of digital gene expression data. *Bioinformatics*. 2010;26:139–140. doi: 10.1093/bioinformatics/btp616
47. Robinson MD, Oshlack A. A scaling normalization method for differential expression analysis of RNA-seq data. *Genome Biol*. 2010;11:R25. doi: 10.1186/gb-2010-11-3-r25
48. Ritchie ME, Phipson B, Wu D, Hu Y, Law CW, Shi W, Smyth GK. limma powers differential expression analyses for RNA-sequencing and microarray studies. *Nucleic Acids Res*. 2015;43:e47. doi: 10.1093/nar/gkv007
49. Law CW, Chen Y, Shi W, Smyth GK. voom: precision weights unlock linear model analysis tools for RNA-seq read counts. *Genome Biol*. 2014;15:R29. doi: 10.1186/gb-2014-15-2-r29
50. Huang DW, Sherman BT, Lempicki RA. Systematic and integrative analysis of large gene lists using DAVID bioinformatics resources. *Nat Protoc*. 2009;4:44–57. doi: 10.1038/nprot.2008.211
51. Gillespie M, Jassal B, Stephan R, Milacic M, Rothfels K, Senff-Ribeiro A, Griss J, Sevilla C, Matthews L, Gong C, et al. The reactome pathway knowledgebase 2022. *Nucleic Acids Res*. 2022;50:D687–D692. doi: 10.1093/nar/gkab1028
52. Karpievitch YV, Nikolic SB, Wilson R, Sharman JE, Edwards LM. Metabolomics data normalization with EigenMS. *PLoS One*. 2014;9:e116221. doi: 10.1371/journal.pone.0116221
53. Xia J, Psychogios N, Young N, Wishart DS. Metaboanalyst: a web server for metabolomic data analysis and interpretation. *Nucleic Acids Res*. 2009;37:W652–W660. doi: 10.1093/nar/gkp356
54. Fleming SJ, Chaffin MD, Arduini A, Akkad AD, Banks E, Marioni JC, Philippakis AA, Ellinor PT, Babadi M. Unsupervised removal of systematic background noise from droplet-based single-cell experiments using CellBender. *Nat Methods*. 2023;20:1323–1335. doi: 10.1038/s41592-023-01943-7
55. Stuart T, Butler A, Hoffman P, Hafemeister C, Papalexi E, Mauck WM, Hao Y, Stoeckius M, Smibert P, Satija R. Comprehensive integration of single-cell data. *Cell*. 2019;177:1888.e21–1902.e21. doi: 10.1016/j.cell.2019.05.031
56. Andreatta M, Carmona SJ. UCell: Robust and scalable single-cell gene signature scoring. *Comput Struct Biotechnol J*. 2021;19:3796–3798. doi: 10.1016/j.csbj.2021.06.043
57. Nestorowa S, Hamey FK, Pijuan Sala B, Diamanti E, Shepherd M, Laurenti E, Wilson NK, Kent DG, Göttgens B. A single-cell resolution map of mouse hematopoietic stem and progenitor cell differentiation. *Blood*. 2016;128:e20–e31. doi: 10.1182/blood-2016-05-716480
58. Tirosh I, Izar B, Prakadan SM, Wadsworth MH, Treacy D, Trombetta JJ, Rotem A, Rodman C, Lian C, Murphy G, et al. Dissecting the multicellular ecosystem of metastatic melanoma by single-cell RNA-seq. *Science*. 2016;352:189–196. doi: 10.1126/science.aad0501
59. Lehtonen JYA, Jokinen JJ, Holmström M, Kupari M. Open chest core needle biopsy of left ventricle in the evaluation of suspected focal myocardial inflammation. *J Thorac Cardiovasc Surg*. 2015;149:e99–102. doi: 10.1016/j.jtcvs.2015.03.016